

Interference analysis for mm-wave picocells

Zhinus Marzi, Upamanyu Madhow, Haitao Zheng
University of California, Santa Barbara, CA 93106, USA
{zh_marzi, madhow}@ece.ucsb.edu, {htzheng}@cs.ucsb.edu

Abstract—Millimeter (mm) wave picocellular networks are a promising approach for delivering the 1000-fold capacity increase required to keep up with projected demand for wireless data: the available bandwidth is orders of magnitude larger than that in existing cellular systems, and the small carrier wavelength enables the realization of highly directive antenna arrays in compact form factor, thus drastically increasing spatial reuse. In this paper, we carry out an interference analysis for mm wave picocells in an urban canyon, accounting for the geometry associated with the sparse multipath characteristic of this band. While we make some modeling simplifications, our analysis provides a strong indication of the very large capacity, of the order of *Terabits/sec per km*, provided by such networks, using system bandwidths of the order of a few GHz.

I. INTRODUCTION

The demand for cellular data is projected to increase 1000-fold by 2020 [1], driven to a large extent by mobile video. Existing cellular systems below 5 GHz are fundamentally constrained by available bandwidth, and are approaching their limits of spectral efficiency. However, millimeter (mm) wave bands (30-300 GHz) offer a potential solution to the capacity crunch faced by mobile operators. There are vast amounts of spectrum available in these bands. In addition, the small wavelengths enable the realization of highly directive antennas in compact form factors, thus producing significant gains in spatial reuse. In this paper, we consider urban picocellular networks using the 60 GHz band, which has 7 GHz of unlicensed spectrum. We conduct an interference analysis that accounts for the unique characteristics of mm wave communication, and use this to provide rough estimates of the attainable network capacity.

We consider picocellular base stations (BSs) deployed on lampposts on each side of the street along an urban canyon (e.g. a typical street in New York City), as depicted in Figure 1. Each BS has two “faces,” facing east and west. Each face may have multiple antenna arrays, each with a large number of elements. Since the carrier wavelength is 5 mm, we note that such arrays are electrically large (many elements) but physically small: for example, an 8×8 array occupies an area of less than a square inch, while a 32×32 array fits within 10 square inches.

The proposed architecture leverages recent progress in development of 60 GHz technology for *indoor* multiGigabit communication, which has resulted in the IEEE 802.11ad standard [2] and the development of low-cost silicon radio frequency integrated circuits (RFICs) [3], [4]. While medium

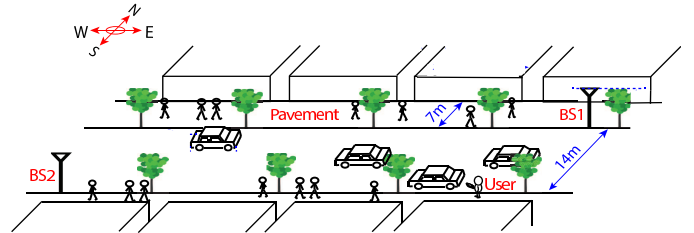


Fig. 1. Picocellular network deployed along an urban canyon

access control would differ considerably for indoor 60 GHz WLANs and outdoor picocellular networks, IEEE 802.11ad physical layer modulation schemes can be used for both.

In prior work involving our research group, we have obtained promising results regarding the basic feasibility of the proposed architecture. Compressive techniques for tracking mobile users with large antenna arrays are developed in [5], [6], which enable tracking both LoS and reflected paths to a mobile. Maintaining path inventories in this fashion enables BSs to seamlessly switch their beams in reaction to blockage due to obstacles in the environment, including the user’s own body. Experimental results with off-the-shelf 60 GHz hardware are presented in [7], demonstrating that the link budget is adequate (in particular, oxygen absorption is not an issue at the relatively short ranges of interest, say 100 m or less, as we increase spatial reuse), that there are multiple paths available to a given user in typical outdoor urban environments, and that inter-cell interference is small, due to the highly directional beams from the BSs to the mobile users.

While there are significant design challenges in realizing the proposed architecture (e.g., see the discussion in [7]), our focus in this paper is to quantify the achievable network capacity as we shrink 60 GHz picocells, assuming that these challenges can be surmounted. Prior work at lower carrier frequencies shows that interference becomes a fundamental limiting factor [8] in picocellular settings, but as we show here, the narrow beams synthesized using large arrays at 60 GHz alleviate this problem.

Contributions: We account for the geometry of the urban canyon in our interference analysis, and obtain the following results.

- We show that the inter-cell interference caused by the main beam directed at the desired user vanishes after a number of cells determined by the heights of the BS and the user.
- We develop analytical expressions for the inter-cell interfer-

ence due to sidelobes, accounting for oxygen absorption and reflections.

- We simulate the statistics of the signal-to-interference-plus-noise ratio (SINR) and attainable data rates under some simple resource management schemes, estimating the attainable network capacity to be of the order of Terabits/sec per km along the canyon, using 2 GHz of spectrum.

Related work: There are a number of prior papers investigating interference in mm wave networks. The effect of directional links on mesh networks is investigated in [9], while indoor environments are considered in [10], [11]. Coverage and attainable data rates in outdoor mm wave networks are investigated in [12] using stochastic geometry models, with BSs, users and obstacles placed in the plane according to Poisson point processes. To the best of our knowledge, ours is the first paper to account for the geometry of an urban canyon to quantify interference and capacity in mm wave networks.

II. SYSTEM MODEL

Figure 1 shows a street segment between adjacent BSs BS1 and BS2. We assume throughout the paper that BSs are placed in a zig-zag pattern, so that immediate neighbors are on opposite sides of the street. Each BS has two antenna arrays, one facing east and the other west. Thus, a user in the street segment shown in Figure 1 is covered by the eastward-facing face of BS2 and the westward-facing face of BS1. Denoting the east-west distance between adjacent BSs as d , the street segment shown can be termed a picocell of width d . Thus, each picocell is covered by one face each from two BSs.

In the next section, we provide a geometric characterization of the inter-cell interference in such a system. Two important simplifications: (a) we ignore interference across parallel urban canyons, as well as interference which might leak from cross streets; (b) we do not consider potential reflections from horizontal ledges. However, while more detailed modeling and simulations are needed to refine the interference and capacity estimates provided here to account for such effects, we expect the qualitative conclusions to remain unchanged.

III. INTER-CELL INTERFERENCE

We investigate the inter-cell interference caused by the main lobe and side lobes separately, since they have different characteristics. Since we consider a large number of antenna elements, the main beam is narrow and is well modeled by a single ray. Side lobes are much weaker, but their directions are difficult to predict, hence we must be more careful in bounding their effect.

A. Main lobe interference

We consider BS antenna arrays with a large number of elements forming a pencil beam towards the desired user. This “desired” beam can be along the LoS, or it can be a single bounce from a wall or the ground (e.g., when steering around an obstacle blocking the LoS). We seek to understand the interference such a beam creates for neighboring BSs. We can use ray tracing for this purpose, given the highly

directive nature of the beam and the limited diffraction at small wavelengths [13].

We assume that each face only creates interference in the direction it is facing. The following theorem proves that the main beam will escape to the sky after a few bounces (Figure 2), assuming that we can ignore the effect of potential reflections from horizontal ledges. Specifically, we bound the distance (from the transmitting BS) over which the main beam can create interference. We denote by h_{max} the maximum height of users, by H_{BS} the height of a BS, and by d the width of a picocell shared among two opposite facing antennas on adjacent BSs (Figure 5).

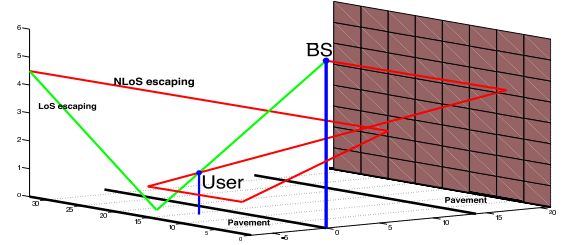


Fig. 2. Mainlobe will escape to sky after a few bounces

Theorem 1. *The maximum range over which the main beam can create interference is bounded by $\frac{H_{BS}+h_{max}}{H_{BS}-h_{max}}d$. Thus, the main beam from a face creates interference for at most $N_{max} = \lceil \frac{H_{BS}+h_{max}}{H_{BS}-h_{max}} \rceil$ adjacent BSs in the direction it is facing.*

In order to prove this theorem, we need to introduce the “virtual” ray. When the “real” (i.e., physical) ray is reflected from any surface (ground or walls), the corresponding virtual ray is the straight line which is the mirror image of the real ray with respect to the reflecting surface. Thus, the direction of the virtual ray is unchanged by the reflection, and it “goes through” walls and the ground. Figure 3 shows an example of a real ray, and the corresponding virtual ray for a single reflection.

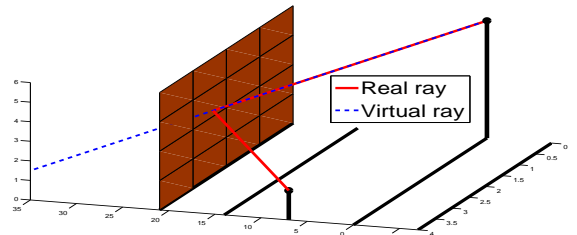


Fig. 3. Real and virtual rays for a wall reflection

Proof. The proof is based on tracing the virtual ray associated with the main beam. Since the BS height is larger

than that of any user, the main beam must go downward to reach the target user. It is easy to see that, in order to maximize the distance over which this beam creates interference, we must have a ground reflection.

Now, suppose that the main beam undergoes a ground reflection. The “real” reflected ray can only go upward, under our assumption that there is no horizontal surface above the ground that can reflect it again to create a downward trajectory. After the ground reflection, the virtual ray is as far below the ground as the real ray is above it (Figure 4). Setting $Z = 0$ as the ground surface, once the virtual ray crosses the $Z = -h_{max}$ plane, the real ray will have gone to a height of more than h_{max} , and can no longer create interference, since a potential victim user has height at most h_{max} .

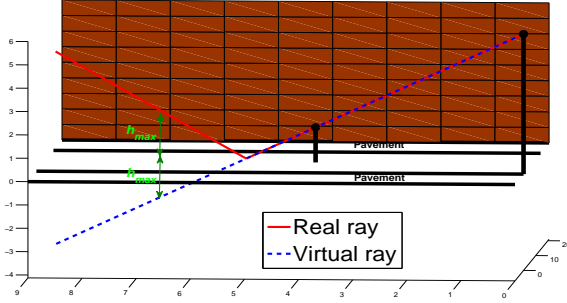


Fig. 4. Ground reflection

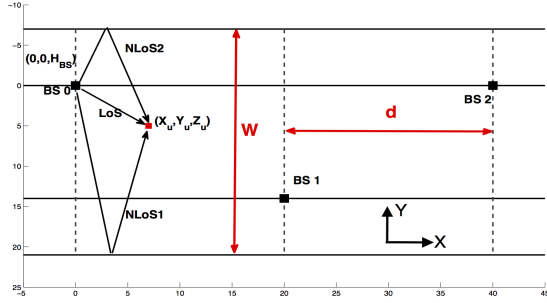


Fig. 5. Problem geometry

Figure 5 provides a bird’s eye view of the urban canyon, and lays out the coordinate system. The line equation of the virtual ray corresponding to the main beam is as follows:

$$\frac{X - X_{BS}}{a} = \frac{Y - Y_{BS}}{b} = \frac{Z - Z_{BS}}{c} \quad (1)$$

where $X_{BS} = Y_{BS} = 0$ and $Z_{BS} = H_{BS}$. As this virtual ray hits $Z = -h_{max}$, the actual ray has gone beyond the region in which it could interfere with users of height at most h_{max} .

$$X = \frac{a}{c}(z - H_{BS})|_{z=-h_{max}} = \frac{a}{c}(-h_{max} - H_{BS}) \quad (2)$$

in which a and c are as follows for LoS and different NLoS paths to the target user, specified in Figure 5.

	LoS	NLoS1	NLoS2	NLoS3
a	X_u	X_u	X_u	X_u
c	$Z_u - H_{BS}$	$Z_u - H_{BS}$	$Z_u - H_{BS}$	$-Z_u - H_{BS}$

Thus, we have the following expression for X :

$$X = \frac{X_u}{\mp Z_u + H_{BS}}(h_{max} + H_{BS}) \quad (3)$$

Since each BS is serving a user inside the immediate picocell, the maximum value of X corresponds to the maximum value of $X_u = d$ (at the edge of coverage for the face), as follows:

$$\max_u X = \frac{d(H_{BS} + h_{max})}{H_{BS} - h_{max}} \quad (4)$$

This is less than or equal to the width of $\frac{H_{BS} + h_{max}}{H_{BS} - h_{max}}$ picocells covered by $\lceil \frac{H_{BS} + h_{max}}{H_{BS} - h_{max}} \rceil$ adjacent BSs. \square

For typical values of $H_{BS} = 6(m)$ and $h_{max} = 2(m)$ employed in our simulations, Theorem 1 implies that the main beam interferes with two adjacent BSs in the direction of the face producing the beam.

B. Sidelobe interference

While the main beam points towards a user inside the picocell, the direction of emission of sidelobes is highly variable, hence it is not possible to limit side lobe interference to a finite number of adjacent picocells. However, as stated in Theorem 2 below, the cumulative sidelobe interference seen within a given picocell is bounded (to a relatively small value), because of the geometric decay (with distance) of the strength of the interference from a distant picocell caused by oxygen absorption and reflection losses, along with the quadratic decay due to path loss. We consider a reference cell 0, and seek to quantify interference from cells $k > 0$ to its east and $k < 0$ from its west.

Denote by P the smallest received power over the desired link, which is given by

$$P = P_{Tx} G_{Tx} G_{Rx} \left(\frac{\lambda}{4\pi L_{max}} \right)^2 e^{-\beta L_{max}} \quad (5)$$

where P_{Tx} , G_{Tx} and G_{Rx} are the transmitter power and the gains of Tx and Rx antenna arrays, respectively. The parameters λ , β and L_{max} denote, respectively, the wavelength, oxygen absorption coefficient (16 dB/km) and maximum length of a link inside a picocell.

Theorem 2. For a user in cell 0, the sidelobe interference due to the BSs $[K, \infty)$ and $(-\infty, K]$ is bounded by $\alpha_K P$, where P is the smallest received power over the desired link.

$$\alpha_K = \frac{\sum_{k=K}^{\infty} I_k + \sum_{n=-\infty}^{-K} I_k}{P} \quad (6)$$

where α_K decays geometrically with K , and is estimated below in (10).

Proof. The total interference introduced by the k th BS to a user inside $cell_0$ known as I_k is given by

$$I_k = \sum_{n=0}^{\infty} I_{k,n} \quad (7)$$

where $I_{k,n}$ is the interference component that travels from the k th BS undergoing n number of bounces before being captured by the Rx antenna array. It can be evaluated as follows:

$$I_{k,n} \approx N_n P_{Tx} (g_{Tx})_{k,n} (g_{Rx})_{k,n} \left(\frac{\lambda}{4\pi r_{k,n}} \right)^2 e^{-\beta r_{k,n}} \left(\frac{1}{l_{k,n}} \right)^n \quad (8)$$

where $(g_{Tx})_{k,n}$, $(g_{Rx})_{k,n}$ and $r_{k,n}$ are the Tx gain, Rx gain and the length of corresponding n times reflected path from k th BS, respectively. Moreover, $\frac{1}{l_{k,n}}$ is the corresponding reflection loss coefficient which depends on the incidence angle and the reflecting surface material. The factor N_n accounts for the number of possible paths (corresponding to different possible ordering of reflectors). While the interference may differ across such paths, we can replace them by a common value because we seek a pessimistic estimate for the interference. By virtue of Theorem 1, for $k > \lceil \frac{H_{BS} + h_{max}}{H_{BS} - h_{max}} \rceil$, $(g_{Tx})_{k,n}$ is the gain of the Tx antenna array outside the main beam.

Note that $r_{k,0}$ is actually the distance between the k th BS and the target user in $cell_0$, and can be roughly approximated by kd . By Pythagoras's theorem, $r_{k,n}$ can be interpreted based on $r_{k,0}$ and W which is the distance between parallel reflectors (buildings or walls):

$$r_{k,n}^2 = r_{k,0}^2 + n^2 W^2 \approx (kd)^2 + (nW)^2 \quad (9)$$

This approximation applies to bounces between two walls. By using arguments similar to those in Theorem 1, there can be at most one ground reflection, and we can ignore its effect on the path length since we are after a pessimistic estimate of the interference. We have at most 4 different possible n -times reflected paths, accounting for whether we have the ground reflection and the order of walls' reflection: $N_n = 4$ for $n > 1$, $N_1 = 3$ and $N_0 = 1$. Thus, the total interference from cells $[K, \infty)$ or $(-\infty, -K]$, divided by P , can be written as follows:

$$\frac{\alpha_K}{2} = \frac{\sum_{k=K}^{\infty} I_k}{P} = \sum_{k=K}^{\infty} \sum_{n=0}^{\infty} \left(N_n \frac{(g_{Tx})_{k,n} (g_{Rx})_{k,n}}{G_{Tx} G_{Rx}} \left(\frac{L_{max}}{r_{k,n}} \right)^2 e^{-\beta(r_{k,n} - L_{max})} \left(\frac{1}{l_{k,n}} \right)^n \right) \quad (10)$$

By substituting (9) above, we obtain

$$\begin{aligned} \frac{\sum_{k=K}^{\infty} I_k}{P} &\leq 4L_{max}^2 e^{\beta L_{max}} \sum_{k=K}^{\infty} \sum_{n=0}^{\infty} \left(\frac{1}{(kd)^2 + (nW)^2} \right) \\ e^{-\beta \sqrt{(kd)^2 + (nW)^2}} \left(\frac{1}{l_{min}} \right)^n &< 4 \sum_{k=K}^{\infty} e^{-\beta kd} \sum_{n=0}^{\infty} \frac{1}{l_{min}^n} \\ &= 4 \frac{e^{-\beta Kd}}{1 - e^{-\beta d}} \frac{l_{min}}{l_{min} - 1} \end{aligned} \quad (11)$$

The same computation holds for interference introduced by cells $(-\infty, -K]$. Thus, α_K defined in equation 6 is bounded and decreases exponentially with increasing K . \square

We now compute α_K using (6) and (8), and plot α_K (dB) versus K in Figure 6. The results are for a 32×32 array at the BS TX, and a 4×4 array at mobile RX. For $K \geq 3$, we only capture interference from sidelobes (Theorem 1), hence $\frac{(g_{Tx})_{k,n}}{G_{Tx}}$ has been substituted by average sidelobe strength relative to the main beam, averaged over the different directions that the main beam can take for users in the picocell. The normalized receive gain $\frac{(g_{Rx})_{k,n}}{G_{Rx}}$, however, is set to the average antenna gain strength in all directions relative to the main beam. We fix the reflection loss at 5 dB, to avoid detailed modeling of material and angle of incidence. This is the smallest reflection loss encountered in outdoor environments for most surfaces, according to measurements reported in [14], hence it is expected to give pessimistic estimates of the interference. We see from Figure 6 that α_K decreases exponentially with K , with higher rate of decrease for wider picocells. We also note that the interference is dominated by the contribution from LoS and first order reflections ($n = 0, 1$); the interference due to these are plotted as dashed lines, and falls on top of the net interference curves obtained by summing over n . Thus, in the simulations in the next section, we restrict attention to $n = 0, 1$.

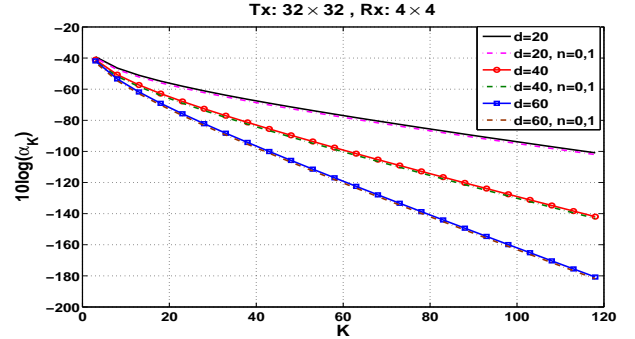


Fig. 6. Normalized Intercell interference

By Theorem 1, if we wish to avoid main beam interference, then $\lceil \frac{H_{BS} + h_{max}}{H_{BS} - h_{max}} \rceil$ adjacent BSs have to coordinate. For $H_{BS} = 6(m)$ and $h_{max} = 2(m)$, this means that every 3 adjacent BSs have to coordinate. Suppose, for example, that we orthogonalize transmissions among such sets of 3 BSs (i.e., with a frequency reuse of 3). Now, from the computations associated with Theorem 2 shown in Figure 6, the cumulative interference caused by sidelobes from BSs beyond this set ($K \geq 3$) is at least 40 dB weaker than the desired received power. Thus, a frequency reuse of 3 leads to very large SINR, so that our spectral efficiency is expected to be bounded only by hardware considerations. This is verified by Monte Carlo simulations in the next section. However, we also show in the next section that such orthogonalization is wasteful. Given the interference reduction due to narrow beams, much larger

network capacity can be obtained (at the expense of a small collision rate) with spatial reuse one.

IV. SIMULATIONS

We now use Monte Carlo simulations for evaluation of inter-cell interference and capacity. We wish to quantify the potential capacity gains from shrinking the picocell width (e.g., down to 20 m). We consider an urban canyon of length 1 km, and consider the interference seen by a typical user in a picocell in the middle of this canyon, which would see the most interference. By virtue of Theorems 1 and 2, we ignore interference coming from outside the 1 km segment.

Since a user in the target picocell can be served by one of two BSs on two different sides, it is unlikely for her body to block the LoS path from both. Furthermore, as we shrink the picocell width, the LoS path slants more steeply downward, hence it is difficult for other obstacles (e.g., pedestrians, cars) to block it. Thus, in our computations, we assume for simplicity that the LoS path is available to the desired user. Of course, both LoS and first order NLoS paths are accounted for when computing interference from other BSs. (as noted earlier, Figure 6 shows that the interference from higher order reflections is negligible in comparison).

Figure 7 is the complementary CDF (CCDF) of the achievable SIR(dB) for 20(m) width picocells. We consider 32×32 Tx and 4×4 Rx antenna arrays, the same settings as for the analytical computations shown in Figure 6. We note that, for a frequency reuse of three, orthogonalizing every three adjacent picocells, the SIR CCDF is consistent with our observation that the main lobe interference has been eliminated (Theorem 1) and sidelobe interference is at least 40 dB weaker than the desired received power as in Figure 6.

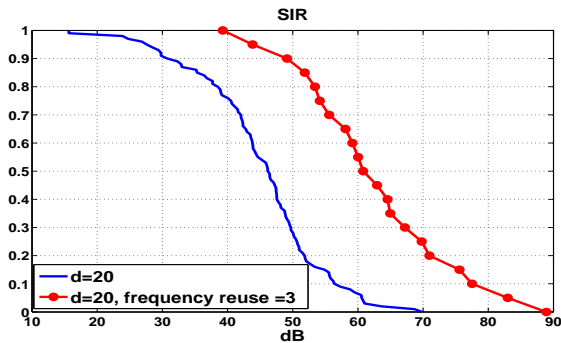


Fig. 7. CCDF of achievable SIR for a 32×32 Tx and 4×4 Rx antenna arrays.

In order to evaluate overall network performance, we now scale back to a smaller 8×8 BS TX array, while still keeping the mobile RX array at 4×4 . These values are chosen because they are close to the current state of the art (32 element arrays are already deployed in commercial 60 GHz products), and it turns out that they suffice to provide full spatial reuse as we scale down cell sizes.

Figure 8 shows the CCDF of the achieved SINR(dB) for three different scenarios: 1) Frequency reuse of one and no

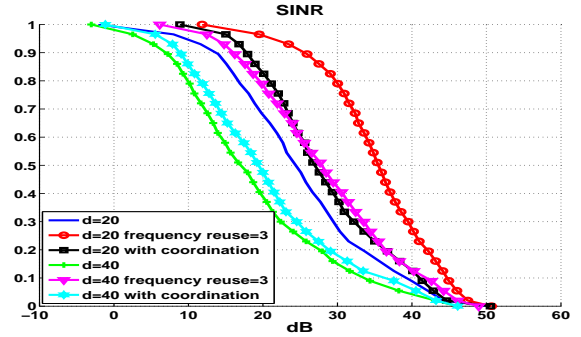


Fig. 8. CCDF of achievable SINR for 8×8 Tx and 4×4 Rx antenna arrays.

coordination: each BS randomly chooses to serve a single user in its own picocell, and hence may interfere with the target user through LoS or NLoS paths. 2) Frequency reuse factor of three, orthogonalizing every set of three adjacent BSs. As already noted, this eliminates main beam interference and drastically reduces sidelobe interference. 3) Multi-User Diversity (MUD) with sets of three adjacent BSs coordinating (minimally). If the SINR of the target user is less than a threshold (set at a fairly high 40 dB in these simulations), out of the two adjacent BSs, the one which introduces the most interference is asked to change its main beam's direction and choose another user to serve (we assume that such a user is always available and is randomly located within the coverage area). If this results in more interference at the target user, the interfering BS reverts to its previously chosen user.

It is possible to consider far more complicated scheduling rules, and optimally choose users to serve among groups of neighboring BSs. However, we leave detailed exploration of medium access control and scheduling to future work, seeking here just to provide some simple capacity benchmarks.

As seen in Figure 8, a frequency reuse of three increases SINR by up to 20dB, mainly because of elimination of main beam interference. However, the corresponding 3X reduction in signaling bandwidth leads to a significant penalty in achievable data rates; see Figure 9. The third scenario, which utilizes multiuser diversity, offers relatively small improvement. This is because our minimal coordination strategy only allows one possible switch. (In addition to simplifying medium access control, another reason for our minimalism is so as not to count on a large pool of users for multiuser diversity within a small picocell.)

We also notice from Figure 8 that the SINR is worse for larger cell widths ($d = 40(m)$) compared to $d = 20(m)$). This might seem surprising, especially because the results in Figure 6 show that sidelobe interference decreases with d . However, the increased interference is due to the main beam from neighboring BSs: for larger cell widths, the target user can be farther away from the BS, and, since the BS height is fixed, the main beam slants down less and therefore interferes with a larger region in the adjacent cell.

In order to estimate capacity, we use the following approx-

imation for the spectral efficiency (in bps/Hz)

$$r = \frac{1}{F} \min(r_{max}, \log(1 + SINR)) \quad (12)$$

where F denotes the frequency reuse factor, and r_{max} the maximum spectral efficiency supported by the system. In our simulations, we (somewhat arbitrarily) set $r_{max} = 6$ bps/Hz, corresponding to uncoded 64QAM (in practice, we would use light coding). Such large constellations may be a stretch with today's hardware, given the phase noise in mm wave radios and the difficulty of high-precision digitization at large bandwidths, but we hope that such hardware limitations would be overcome in the future.

The achievable data rate for a BS face is therefore given by $R_{picocell} = rB$, where B denotes the available system bandwidth. Figure 9 shows the achievable data rates in a picocell for system bandwidth $B = 2$ GHz. We do not account for excess bandwidth in our data rate estimates. While frequency reuse of 3 (which could be implemented via either time division or frequency division) yields more deterministic performance, the achievable rate is about 4 Gbps, which is significantly smaller than the 90% availability rate of 12 Gbps for our third scheme (full reuse, minimal coordination). This data rate corresponds to saturation of spectral efficiency at $r_{max} = 6$ bps/Hz, and would scale down if we used smaller constellations (e.g., 4 Gbps for QPSK). Thus, as long we allow a small outage probability for occasional collisions across adjacent picocells, hardware rather than interference is the bottleneck.

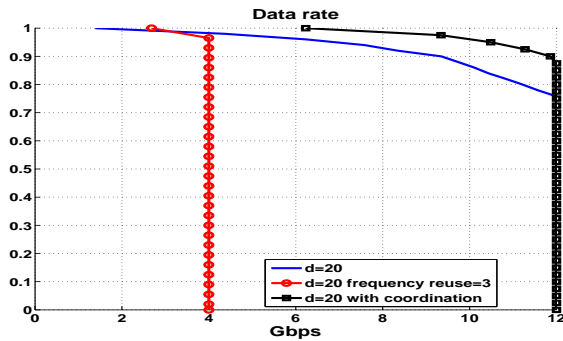


Fig. 9. CCDF of achievable data rates over 2GHz bandwidth for 8×8 Tx and 4×4 Rx antenna arrays

We can now estimate the capacity of a picocellular network deployed over a length of urban canyon. Since each BS has two faces, there are twice the number of active links as BSs. For $d = 20(m)$, there are 50 BSs per km, and hence 100 active links. According to Figure 9, each link can support 12 Gbps at 90% availability, so that the entire network capacity is estimated at 1.2 Tbps per km using 2 GHz of spectrum.

V. CONCLUSIONS AND FUTURE WORK

Our geometric interference analysis shows that the pencil beams formed by large antenna arrays indeed permit aggressive spatial reuse, allowing dense BS deployment (e.g., with

20 m spacing) in urban environments. While more detailed modeling and simulations are required to account for effects ignored here (e.g., inter-canyon interference, cross-street interference, horizontal ledges), we expect our qualitative conclusions of Tbps/km capacity with a few GHz of bandwidth to continue to hold. Furthermore, it is possible to obtain even larger gains by using multiple antenna arrays on each BS face. Of course, we must then address the problem of *intra-cell* interference, which may involve more sophisticated resource management strategies than the relatively simple approaches considered here: for example, MAC layer approaches for admission control and coordination to choose least interfering users, or PHY layers approaches such as nullforming. Finally, while the analysis presented here testifies to the immense potential of mm wave picocellular networks, significant challenges lie ahead in engineering such networks, including user tracking, BS coordination and backhaul (see discussion in [7]).

REFERENCES

- [1] <http://www.techjournal.org/2011/09/mobile-broadband-useage-is-set-to-explode-infographic>.
- [2] http://www.ieee802.org/11/Reports/tgad_update.htm.
- [3] <http://www.siliconimage.com/news/releasedetails.aspx?id=649>.
- [4] http://news.cnet.com/8301-30685_3-57326718-264/wilocity-60ghz-wireless-revolution-begins-at-ces/.
- [5] D. Ramasamy, S. Venkateswaran, and U. Madhow, "Compressive adaptation of large steerable arrays," in *Information Theory and Applications Workshop (ITA), 2012*, pp. 234–239, feb. 2012.
- [6] D. Ramasamy, S. Venkateswaran, and U. Madhow, "Compressive tracking with 1000-element arrays: a framework for multi-gbps mm wave cellular downlinks," in *Proc. 50th Annual Allerton Conf. on Commun., Control and Computing (Allerton 2012)*, October 2012. to appear.
- [7] Y. Zhu, Z. Zhang, Z. Marzi, C. Nelson, U. Madhow, B. Y. Zhao, and H. Zheng, "Demystifying 60ghz outdoor picocells," in *Proceedings of the 20th Annual International Conference on Mobile Computing and Networking, MobiCom '14*, (New York, NY, USA), pp. 5–16, ACM, 2014.
- [8] D. Ramasamy, R. Ganti, and U. Madhow, "On the capacity of picocellular networks," in *Information Theory Proceedings (ISIT), 2013 IEEE International Symposium on*, pp. 241–245, July 2013.
- [9] S. Singh, R. Mudumbai, and U. Madhow, "Interference analysis for highly directional 60-ghz mesh networks: The case for rethinking medium access control," *Networking, IEEE/ACM Transactions on*, vol. 19, pp. 1513–1527, Oct 2011.
- [10] M. Park and P. Gopalakrishnan, "Analysis on spatial reuse, interference, and mac layer interference mitigation schemes in 60 ghz wireless networks," in *Ultra-Wideband, 2009. ICUWB 2009. IEEE International Conference on*, pp. 1–5, Sept 2009.
- [11] A. Maltsev, R. Maslennikov, A. Maltsev, A. Khoryaev, and M. Shilov, "Performance analysis of spatial reuse mode in millimeter-wave wpan systems with multiple links," in *Personal, Indoor and Mobile Radio Communications, 2008. PIMRC 2008. IEEE 19th International Symposium on*, pp. 1–4, Sept 2008.
- [12] T. Bai and R. W. H. Jr., "Coverage and rate analysis for millimeter wave cellular networks," *CoRR*, vol. abs/1402.6430, 2014.
- [13] M. Rasekh, A. Shishegar, and F. Farzaneh, "A study of the effect of diffraction and rough surface scatter modeling on ray tracing results in an urban environment at 60 ghz," in *Millimeter-Wave and Terahertz Technologies (MMWaTT), 2009 First Conference on*, pp. 27–31, Dec 2009.
- [14] B. Langen, G. Lober, and W. Herzig, "Reflection and transmission behaviour of building materials at 60 ghz," in *Personal, Indoor and Mobile Radio Communications, 1994. Wireless Networks - Catching the Mobile Future., 5th IEEE International Symposium on*, pp. 505–509 vol.2, Sep 1994.